Research Paper

Baicalein ameliorates osteoporosis via AKT/FOXO1 signaling

Pan Cai[1,*], Yan Lu[2,*], Zhifeng Yin[3], Xiuhui Wang[1], Xiaoxiao Zhou[1], Zhuokai Li[1]

[1]Department of Orthopedics, Shanghai University of Medicine and Health Sciences Affiliated Zhoupu Hospital, Shanghai, China
[2]Department of Laboratory Medicine, Shanghai University of Medicine and Health Sciences Affiliated Zhoupu Hospital, Shanghai, China
[3]Department of Orthopedics, Shanghai Zhongye Hospital, Shanghai 200941, China
*Equal contribution

Correspondence to: Zhuokai Li; **email:** zp_caip@sumhs.edu.cn
Keywords: baicalein, osteoporosis, KEGG, AKT
Received: February 22, 2021 **Accepted:** May 18, 2021 **Published:** July 1, 2021

ABSTRACT

In this study, we used bioinformatics and an *in vitro* cellular model of glucocorticoid-induced osteoporosis to investigate mechanisms underlying the beneficial effects of baicalein (BN) against osteoporosis. STITCH database analysis revealed 30 BN-targeted genes, including *AKT1, CCND1, MTOR*, and *PTEN*. Functional enrichment analysis demonstrated that BN-targeted genes were enriched in 49 Kyoto Encyclopedia of Genes and Genomes (KEGG) pathways. MIRWALK2.0 database analysis identified 110 enriched KEGG pathways related to osteoporosis. A Venn diagram demonstrated that 26 KEGG pathways were common between osteoporosis and BN-targeted genes. The top 5 common KEGG pathways were prostate cancer, bladder cancer, glioma, pathways in cancer, and melanoma. BN-targeted genes in the top 5 shared KEGG pathways were involved in PI3K-AKT, MAPK, p53, ErbB, and mTOR signaling pathways. In addition, glucocorticoid-induced osteoporosis in MC3T3-E1 cells was partially reversed by BN through inhibition of AKT, which, by upregulating FOXO1, enhanced expression of bone turnover markers (ALP, OCN, Runx2, and Col 1) and extracellular matrix mineralization. These findings demonstrate that BN suppresses osteoporosis via an AKT/FOXO1 signaling pathway.

INTRODUCTION

Osteoporosis is a metabolic bone disease commonly diagnosed in the elderly [1]. Chronic osteoporosis is manifest by progressive brittleness of bones and greater incidence of non-stress fractures because of excessive bone resorption, low bone mineral density, and deterioration of bone micro-structure [2, 3]. Several genetic and environmental factors, such as Vitamin D deficiency and low estrogen levels, contribute to the progression of osteoporosis [4]. However, molecular mechanisms underlying osteoporosis remain unclear.

Baicalein (BN) is one of the most abundant flavonoid in *Scutellaria baicalensis*, which is widely used in Chinese herbal medicine for various ailments [5]. For example, BN reduces cerebrovascular resistance, improves cerebral blood circulation, and prevents platelet agglutination [5]. BN is clinically used for treatment of paralysis in patients with cerebrovascular disease [6]. The beneficial effects of BN on osteoporosis have also been reported. For example, BN acts as a lipoxygenase inhibitor and increases bone formation in osteoporosis model mice [7]. Moreover, BN promotes osteoblastic differentiation of MC3T3-E1 cells via protein kinases and transcription factors such as P-4E/BP1 and P-S6K1 [8]. However, the molecular mechanisms underlying the therapeutic effects of BN on osteoporosis are not clear.

Bioinformatics analysis has been widely used to unravel molecular and cellular mechanisms of several human

diseases [9–11]. Therefore, in this study, we performed comprehensive bioinformatics analysis and *in vitro* experiments in the cellular model of glucocorticoid-induced osteoporosis (GIO) to identify molecular mechanisms underlying the therapeutic effects of BN in osteoporosis.

RESULTS

BN-targeted genes and the interaction network

We identified 30 baicalein-targeted genes belonging to three shells based on STITCH database analysis. The interaction network between these 30 baicalein-targeted genes is shown in Figure 1A. The first shell contained genes such as *CYP1A2*, *CYP3A4*, *CDK4*, *MMP2*, *AKT1*, *MMP9*, *MAPK1*, *PLAU*, *ALOX12*, and *ALOX15* and were probably the direct targets of baicalein. The second shell included genes such as *MTOR*, *RICTOR*, *TIMP2*, *RB1*, *CDKN1A*, *CDKN1B*, *CDKN2A*, *CCND3*, *FOXO1*, and *CCND1*. The third shell included genes such as *MAP2K1*, *NOS3*, *ILK*, *HSP90AA1*, *PTEN*, *FOXO3*, *MDM2*, *CDKN2C*, *CCND2*, and *CDKN2B*. The network of baicalein-targeted genes based on interaction weights is shown in Figure 1B. *AKT1*, *CCND1*, *MTOR*, and *PTEN* showed the highest interaction weights among the 30 baicalein-targeted genes.

PPI network of BN-related genes

The protein-protein interaction (PPI) network of BN-related genes using Cytoscape (Figure 2A). The baicalein-targeted genes were ranked according to degree values (Figure 2B). The top ten genes based on degree values were *AKT1*, *CCND1*, *PTEN*, *MTOR*, *CDK4*, *CDKN1A*, *CDKN1B*, *CDKN2A*, *FOXO3*, and *FOXO1*.

Identification of shared KEGG pathways between BN-targeted genes and osteoporosis

We identified 49 enriched KEGG pathways ($p < 0.05$) by performing functional enrichment analysis of baicalein-targeted genes using DAVID. Furthermore, we identified 110 enriched KEGG pathways associated with human osteoporosis using the miRWalk2.0 database. We further identified 26 common KEGG pathways between osteoporosis and baicalein-targeted genes using the Venn diagram (Figure 3). Among these, prostate cancer, bladder cancer, glioma, pathway in cancer, and melanoma were the top five common KEGG pathways (Table 1).

Identification of baicalein-targeted hub genes

Functional enrichment analysis of BN-targeted genes is shown in Figure 4A. Among the 30 BN-targeted genes,

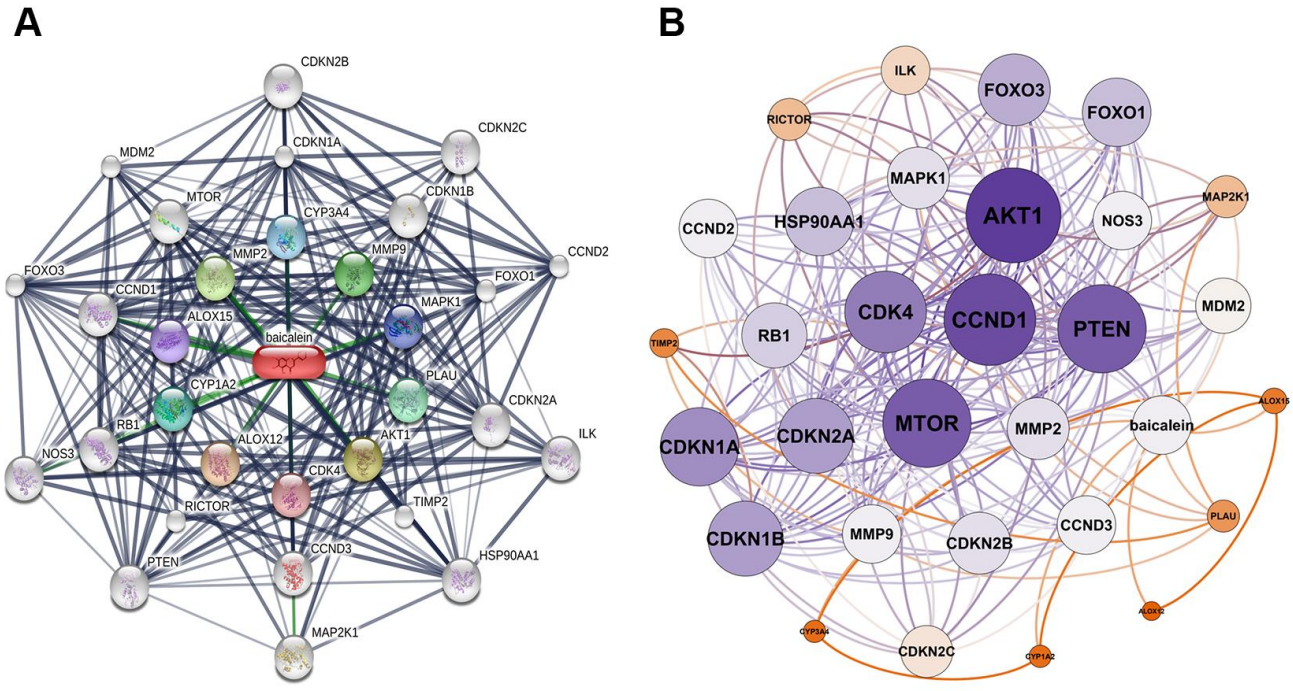

Figure 1. Identification of baicalein-targeted genes. (**A**) Identification of 30 baicalein-targeted genes using STITCH database. (**B**) Weighted interaction network analysis of baicalein-targeted genes using the STITCH database. The weights of *AKT1, CCND1, MTOR*, and *PTEN* were highest among BN-targeted genes.

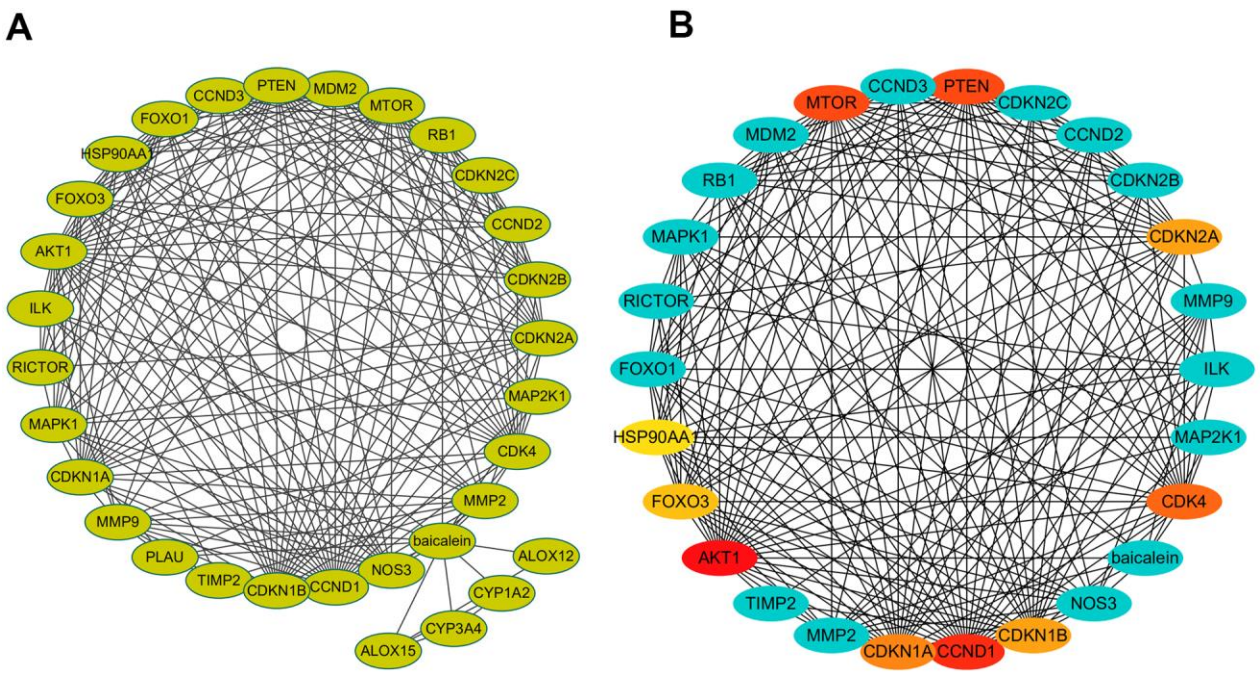

Figure 2. PPI network of baicalein-targeted genes. (**A**) PPI network of baicalein-targeted genes constructed using Cytoscape. (**B**) A list of baicalein-targeted genes in the PPI network ranked by degree connectivity. As shown, the top ten baicalein-targeted genes by degree connectivity were AKT1, CCND1, PTEN, MTOR, CDK4, CDKN1A, CDKN1B, CDKN2A, FOXO3, and FOXO1.

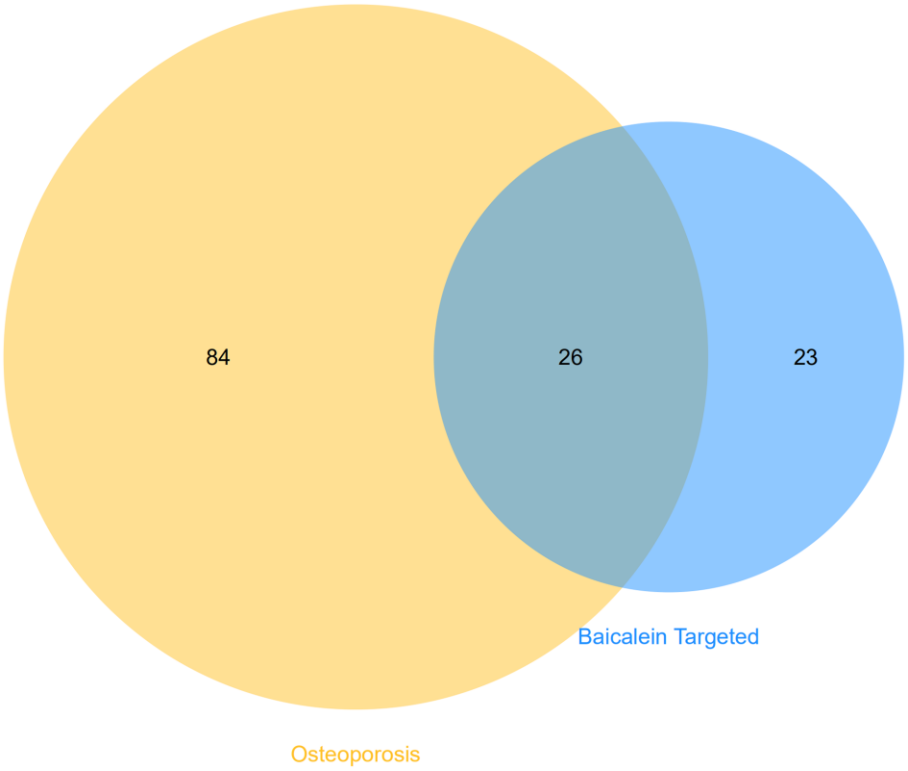

Figure 3. Identification of shared KEGG pathways related to baicalein-targeted genes and osteoporosis. Venn diagram shows 26 common KEGG pathways by intersecting those related to baicalein-target genes (n=49 KEGG pathways) and osteoporosis (n=110 KEGG pathways).

Table 1. Top five KEGG pathway and involved genes.

Term	KEGG pathway	Baicalein-target genes	*Adj P*-value
hsa05215	Prostate cancer	RB1, CDKN1A, MAP2K1, HSP90AA1, CDKN1B, CCND1, PTEN, MDM2, MAPK1, AKT1, FOXO1, MTOR	8.67E-13
hsa05219	Bladder cancer	RB1, CDKN1A, MAP2K1, CCND1, CDKN2A, CDK4, MMP2, MDM2, MAPK1, MMP9	8.67E-13
Hsa05214	Glioma	RB1, CDKN1A, MAP2K1, CCND1, CDKN2A, CDK4, PTEN, MDM2, MAPK1, AKT1, MTOR	8.67E-13
hsa05200	Pathways in cancer	RB1, CDKN1A, MAP2K1, CDKN2B, HSP90AA1, CDKN1B, CDKN2A, MMP2, PTEN, MMP9, FOXO1, MTOR, CCND1, CDK4, MDM2, AKT1, MAPK1	3.17E-12
Hsa05128	Melanoma	RB1, CDKN1A, MAP2K1, CCND1, CDKN2A, CDK4, PTEN, MDM2, MAPK1, AKT1	6.22E-11

AKT1, *CCND1*, *PTEN*, *MTOR*, *CDK4*, *CDKN1A*, *CDKN1B*, *CDKN2A*, *FOXO1*, *HSP90AA1*, *RB1*, *MMP2*, *MAPK1*, *CDKN2B*, *MMP9*, *MDM2*, and *MAP2K1* were involved in the top five KEGG pathways. Furthermore, we identified *CCND1*, *CDKN1A*, *RB1*, *MAPK1*, *MDM2*, and *MAP2K1* were identified as hub genes (Figure 4B). The FDR values, gene counts, and rich factors are shown in Figure 4C. The KEGG pathway, hsa05200: pathways in cancer, showed the highest FDR value, rich factor, and gene numbers (Figure 4C).

Analysis of KEGG pathways related to BN-targeted genes

The top 5 baicalein-targeted KEGG pathways were associated with apoptosis inhibition, cell cycle progression, impaired G1 and G2 cell cycle arrest, genomic instability, tumor growth, cell growth and proliferation, angiogenesis, G1/S cell cycle progression, uncontrolled proliferation, and increased survival (Figure 5). This suggested that baicalein regulated osteogenesis through PI3K-AKT, MAPK, p53, ErbB, and mTOR signaling pathways.

BN partially reverses GIO through suppression of AKT expression

We then analyzed AKT phosphorylation levels in MC3T3-E1 cells treated with different concentrations of baicalein (1 μM, 10 μM, and 100 μM) by ELISA. BN treatment significantly reduced p-AKT levels in MC3T3-E1 cells; p-AKT levels were significantly

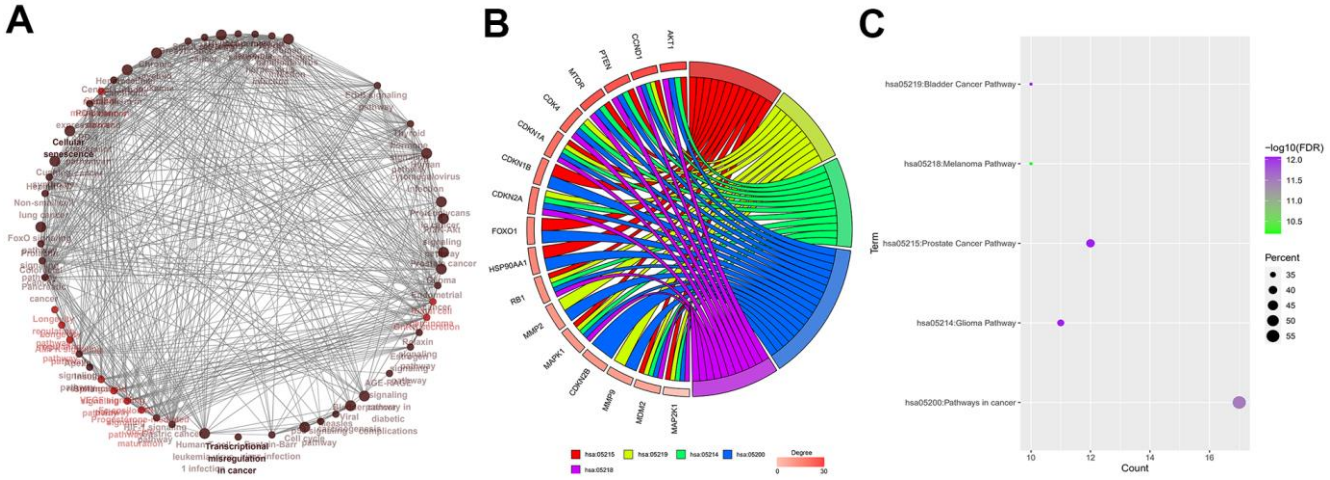

Figure 4. Identification of hub genes. (**A**) Relationship and interactions between baicalein-targeted genes in the top 5 enriched KEGG pathways. (**B**) Functional enrichment analysis results of baicalein-targeted genes. *CCND1, CDKN1A, RB1, MAPK1, MDM2*, and *MAP2K1* were common to all the top five shared KEGG pathways and were designated as hub genes. The top five genes based on degree connectivity were *AKT1, CCND1, PTEN, MTOR*, and *CDK4*. (**C**) The FDR values, gene numbers, and rich factor values (ratio of the number of enriched DEGs in the KEGG pathway category compared to the total number of genes in that category) of the top five shared KEGG pathways.

lower in the 10 μM BN-treatment group compared to the 1 μM and 100 μM BN-treatment groups (Figure 6A). QRT-PCR analysis results showed that the GIO treatment significantly decreased the expression levels of bone turnover markers such as ALP, OCN, Runx2, and Col 1 in MC3T3-E1 cells, but these effects were partially reversed by BN (Figure 6B–6E). Furthermore, ALP staining assay results showed that BN partially rescued impaired extracellular matrix mineralization in GIO-treated MC3T3-E1 cells (Figure 6F, 6G).

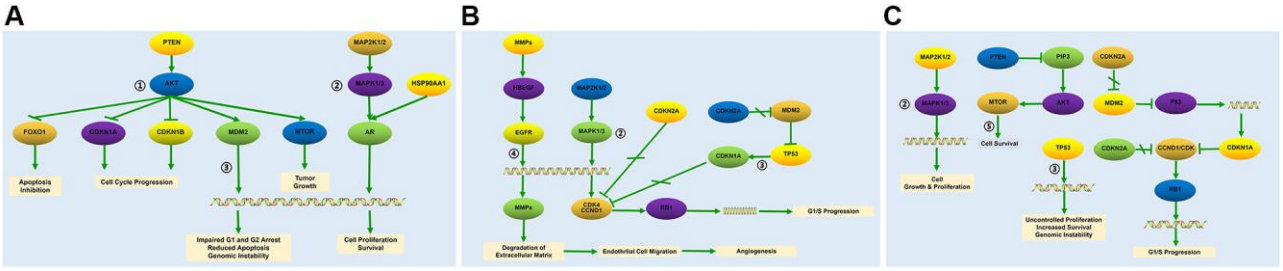

Figure 5. Baicalein-targeted genes in the top three KEGG pathways. The list of baicalein-targeted genes among (**A**) PI3K-AKT, MAPK, and p53 signaling pathway genes enriched in prostate cancer; (**B**) MAPK, p53, and ErbB signaling pathway genes enriched in bladder cancer, and (**C**) MAPK, p53, and mTOR signaling pathway genes enriched in pathways in cancer.

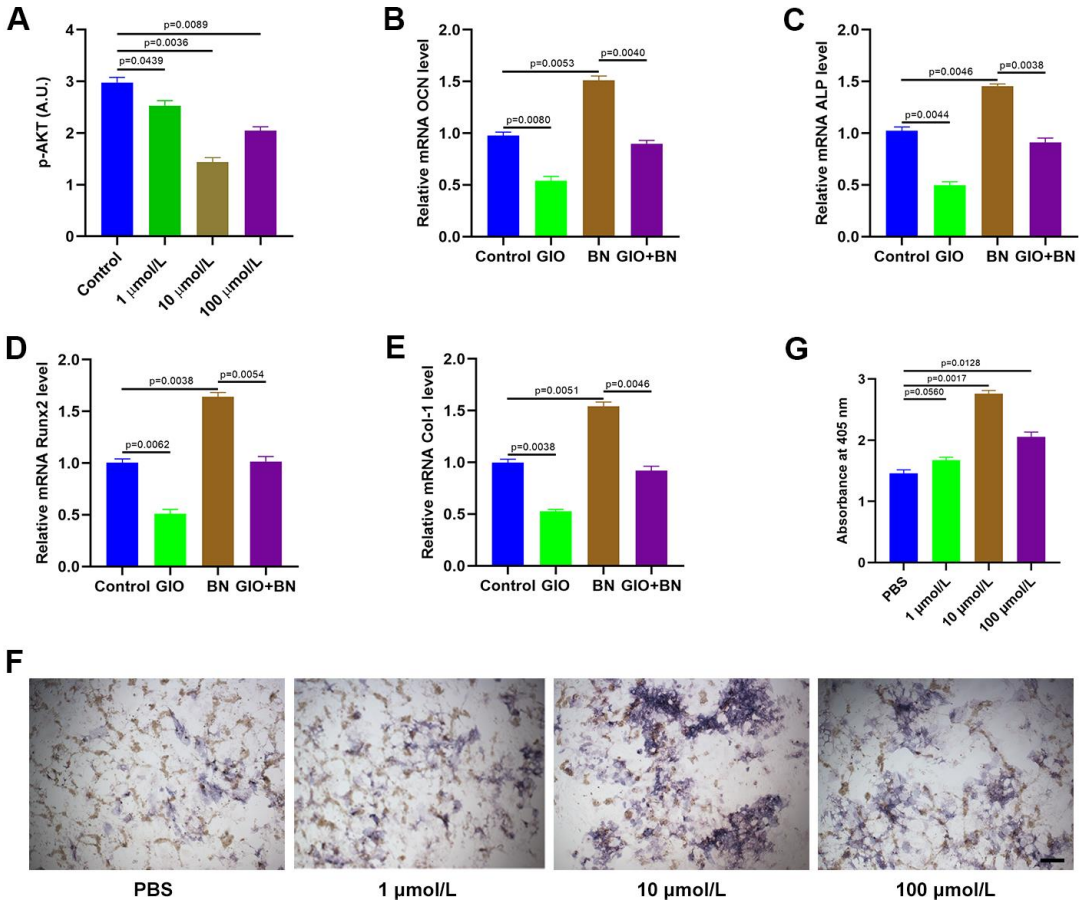

Figure 6. BN treatment partially reverses GIO by suppressing AKT. (**A**) ELISA analysis shows phospho-AKT levels in GIO-induced MC3T3-E1 cells treated with BN (1μM, 10 μM, and 100 μM). (**B**–**E**) QRT-PCR analysis shows expression levels of bone turnover markers (ALP, OCN, Runx2, and Col 1) in GIO model MC3T3-E1 cells treated with BN (10 μM, 10 μM, and 100 μM BN). (**F**, **G**) ALP staining results of GIO model MC3T3-E1 cells treated with BN (1μM, 10 μM, and 100 μM). The data are represented as means±SD of at least 3 independent experiments.

BN regulates osteogenesis via AKT/FOXO1 signaling

QRT-PCR analysis showed that expression of FOXO1 was significantly increased in BN-treated MC3T3-E1 cells; FOXO1 levels were highest in the 10 μM BN-treatment group (Figure 7A). Furthermore, qRT-PCR analysis confirmed that AKT levels were significantly reduced in AKT-siRNA-transfected MC3T3-E1 cells compared to the corresponding controls (Figure 7B). AKT silencing significantly increased FOXO1 levels in MC3T3-E1 cells **(**Figure 7C). QRT-PCR analysis

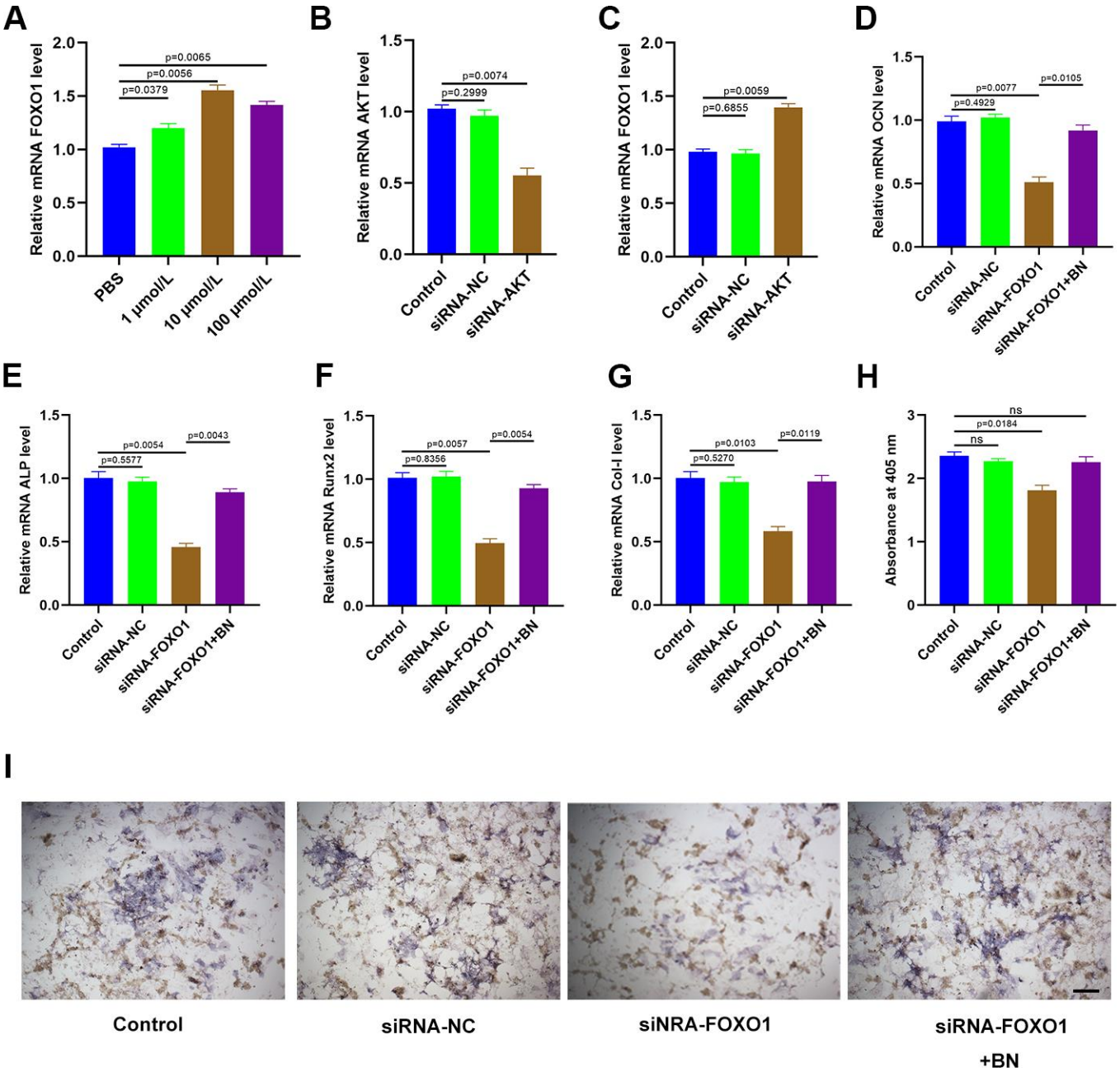

Figure 7. BN regulates osteogenesis via AKT/FOXO1 signaling. (**A**) QRT-PCR analysis shows FOXO1 levels in GIO model MC3T3-E1 cells treated with BN (1μM, 10 μM, and 100 μM). (**B**) QRT-PCR analysis shows AKT mRNA levels in control-siRNA- and AKT siRNA-transfected MC3T3-E1 cells. (**C**) QRT-PCR analysis shows the levels of FOXO1 in control-siRNA- and AKT siRNA-transfected GIO model MC3T3-E1 cells treated with BN (1μM, 10 μM, and 100 μM). (**D**–**G**) QRT-PCR analysis shows the levels of bone turnover markers (ALP, OCN, Runx2, and Col 1) in control-siRNA- and AKT siRNA-transfected GIO model MC3T3-E1 cells treated with BN (1μM, 10 μM, and 100 μM). (**H**, **I**) ALP staining results of control-siRNA- and AKT siRNA-transfected GIO model MC3T3-E1 cells treated with BN (1μM, 10 μM, and 100 μM). The data are shown as means±SD of 3 independent experiments.

showed that FOXO1 silencing significantly reduced expression levels of the bone turnover markers (ALP, OCN, Runx2, and Col 1) in GIO-treated MC3T3-E1 cells, but these effects were partially reversed by BN treatment (Figure 7D–7G). ALP staining results showed that BN treatment partially rescued impaired extracellular matrix mineralization in GIO-treated FOXO1-silenced MC3T3-E1 cells (Figure 7H, 7I).

DISCUSSION

Osteoporosis is a chronic metabolic bone disorder observed commonly in aged individuals, and is characterized by low bone mineral density, increased brittleness of bone, damaged bone micro-structure, and significant increase in the number of non-stress fractures [12]. BN is one of the most abundant flavonoids in *Scutellaria baicalensis* and is widely used in Chinese herbal medicine to treat various human diseases for centuries. [13]. BN promotes osteogenic differentiation and bone formation [14–16], but the molecular mechanisms underlying the beneficial effects of BN on osteoporosis are not clear. Pathogenetic mechanisms underlying several human diseases have been discovered through bio-informatics analyses of microarray data and whole-genome sequencing studies [17].

In the present study, we identified 110 KEGG pathways that were associated with differentially expressed genes (DEGs) in human osteoporosis and 49 KEGG pathways associated with BN-targeted genes. PI3K-AKT, MAPK, p53, ErbB, and mTOR signaling pathways were the top five shared KEGG pathways among these two groups.

Previous studies have shown that BN-targeted genes in the PI3K-AKT signaling pathway were associated with osteogenesis [18, 19]. Many studies have shown that PI3K-AKT signaling pathway plays a significant role in osteoporosis [20, 21]. For an example, a recent study demonstrated that inhibition of PI3K-AKT signaling pathway delayed osteoporosis progression in post-menopausal women by suppressing inflammation and formation of osteoclasts [22]. Xiao et al demonstrated that inhibition of miR-148a ameliorated ovariectomy-induced osteoporosis via PI3K-AKT signaling pathway [23]. In the present study, we showed that BN significantly suppressed AKT expression and activation in MC3T3-E1 cells. BN treatment also stimulated the expression of bone turnover markers and enhanced extracellular matrix mineralization in GIO-induced MC3T3-E1 cells. These results suggested that the BN treatment suppresses osteoporosis via AKT.

FOXO family of transcription factors such as FOXO1, FOXO3, FOXO4, and FOXO6 play a crucial role in cellular defense mechanisms against oxidative stress [24]. Liao et al reported that FOXO1 knockdown decreased osteoblast differentiation by suppressing the expression of antioxidant enzymes, manganese super-oxide dismutase and catalase, thereby increasing the levels of reactive oxygen species [25]. Feng et al demonstrated that inhibition of PI3K-AKT signaling pathway significantly increased FOXO1 transcriptional activity, which suppressed osteoporosis by enhancing antioxidant mechanisms [26]. In our study, we demonstrated that BN promoted expression of FOXO1 by suppressing AKT. We also observed that BN treatment and AKT silencing improved osteogenic differentiation of GIO-induced MC3T3-E1 cells by increasing FOXO1 expression. Therefore, our results demonstrate that BN treatment suppresses osteoporosis via AKT/FOXO1 signaling pathway. Future studies are required to confirm our findings *in vivo* and further investigate mechanisms underlying the beneficial effects of BN on osteogenesis.

MATERIALS AND METHODS

Cell culture and transfection

The murine pre-osteoblast cell line, MC3T3-E1, was a kind donation from the Shanghai University of Medicine and Health Sciences (Shanghai, China). MC3T3-E1 cells were grown in α-MEM medium (SH30265.01B; Hyclone) containing 10% fetal bovine serum (FBS; Gibco) and 1% penicillin and streptomycin at 37° C, 5% CO_2, and 95% humidity. MC3T3-E1 cells up to five passages were used for experiments. The cells were transfected with 50 nM AKT siRNA, 50 nM FOXO1 siRNA and their corresponding control siRNAs using lipofectamine 3000. MC3T3-E1 cells were treated with 100 μM dexamethasone (CAS: 50-02-2, purity: >98%; ACMEC, Shanghai, China) for 7 days to induce the cellular GIO model. The cells were treated with 1 μM, 10 μM, and 100 μM baicalein (Cat. No. HY-N0196-100 mg; MedChemExpress) for various time points as indicated.

Quantitative real-time PCR (qRT-PCR)

Total RNA was extracted using TRIzol according to manufacturer's instructions. Then, cDNA synthesis was performed using the one-step Prime Script miRNA cDNA synthesis kit. Then, qPCR analysis was performed using SYBR Premix Ex TaqII (TaKaRa, Japan) in the Thermal Cycler C-1000 Touch system (CFX Manager, 10021377; Bio-Rad, USA). The expression levels of various genes were determined using the $2^{-\Delta\Delta Ct}$ method and normalized to GAPDH. The primers used for qPCR analysis were as follows: AKT-forward, 5′- ATGAGCGACGTGGCTATTGT- 3′, AKT-reverse, 5′- GAGGCCGTCAGCCACAGTCT- 3′;

FOXO1-forward, 5′- AGGGTTAGTGAGCAGGTTACAC- 3′,
FOXO1-reverse, 5′- TGCTGCCAAGTCTGACGAAA- 3′;
ALP-forward, 5′- TGACTACCACTCGGGTGAACC- 3′,
ALP-reverse, 5′- TGATATGCGATGTCCTTGCAG- 3′;
OCN-forward, 5′- TTCTGCTCACTCTGCTGACCC- 3′,
OCN-reverse, 5′- CTGATAGCTCGTCACAAGCAGG- 3′;
Runx2-forward, 5′- CGCCACCACTCACTACCACAC- 3′,
Runx2-reverse,5′- TGGATTTAATAGCGTGCTGCC- 3′;
Col-1-forward, 5′- AACTTTGCTTCCCAGATGTCC- 3′,
Col-1-reverse, 5′- AGCCTCGGTGTCCCTTCA- 3′;
GAPDH-forward, 5′- GAAGGTCGGTGTGAACGGATTTG- 3′,
GAPDH-reverse, 5′- CATGTAGACCATGTAGTTGAGGTCA- 3′.

ELISA

MC3T3-E1 cells were grown for 48 h in serum-free medium. The concentration of phospho-AKT in each group of cells was measured using the ELISA kit according to manufacturer's instructions. The colorimetric values were normalized to total cell numbers in each well. Then, the phospho-AKT levels in each sample were calculated using the standard curve.

ALP staining

MC3T3-E1 cells were washed twice with PBS and then fixed with 10% formalin for 15 minutes. Then, the cells were processed using the ALP color-development kit according to manufacturer's instructions and the color development was performed by incubating cells with BCIP/NBT liquid substrate for 24 hours. Absorbance was measured at 405 nm in a plate reader. The experiments were performed in triplicate.

Identification of BN-target genes and construction of PPI network

We identified baicalein-targeted genes and constructed the protein-protein interaction (PPI) network between them using the Search Tool for Interacting Chemicals (STITCH) database [27]. We analyzed the PPI network of baicalein-targeted genes using the Cytoscape 3.7.2 version software [28] and measured the degree, betweenness, and closeness of each gene in the network. The hub genes were identified based on the degree analysis using the cytoHubba plugin. Cytoscape plug-in ClueGO was used to identify enriched KEGG pathways representing the baicalein-targeted genes and the relationship between them. The KEGG pathway enrichment results were visualized using the ggplot2.7 package.

Identification of shared KEGG pathways between BN-targeted genes and osteoporosis

MiRWalk2.0 software [29] was used to retrieve human osteoporosis-related KEGG pathways using $p<0.05$ as the threshold parameter. VennDiagram (http://www.ehbio.com/ImageGP/index.php/Home/Index/index.html) was then used to identify shared KEGG pathways between human osteoporosis and baicalein-targeted genes.

Identification of hub genes

GOplot R package [30] was used to visualize functional enrichment analysis of KEGG pathways enriched with baicalein-targeted genes and identified hub genes from among the top five shared KEGG pathways between baicalein-targeted genes and osteoporosis.

Identification of KEGG pathways related to BN-targeted genes

We selected the top 5 shared KEGG pathways with the smallest p values and used ScienceSlides to schematically represent KEGG pathways related to baicalein-targeted genes, the hub genes and their related mechanisms of action.

Statistical analysis

The data are represented as means ± SD. Prism 8.0 software was used for all statistical analyses. One-way analysis of variance with Tukey's post hoc test was used to compare three or more groups of data. Two-tailed Student's test was used to compare data between two groups. $P < 0.05$ was considered statistically significant.

AUTHOR CONTRIBUTIONS

PC conceived and designed the study; PC, YL and ZL supervised the study; PC and YL performed bioinformatics analysis and experiments; ZY, XW and XZ analyzed the data; XZ and ZL provided advice and technical assistance; PC, YL and ZL wrote the manuscript. All authors approved the final manuscript.

CONFLICTS OF INTEREST

The authors declare that they have no conflicts of interest.

FUNDING

This study was supported by grants from The Construction of Key Medical Specialties of Shanghai

(Grant No. ZK2019-B05), The Shanghai Pudong New Area Health system Key Discipline group (Grant No. PWZxq2017-12), and The Featured Clinical Discipline Project of Shanghai Pudong (Grant No. PWYts2018-02).

REFERENCES

1. Lewis JR, Voortman T, Ioannidis JP. Evaluating and Strengthening the Evidence for Nutritional Bone Research: Ready to Break New Ground? J Bone Miner Res. 2021; 36:219–26. https://doi.org/10.1002/jbmr.4236 PMID:33503301

2. Mohd Ramli ES, Sukalingam K, Kamaruzzaman MA, Soelaiman IN, Pang KL, Chin KY. Direct and Indirect Effect of Honey as a Functional Food Against Metabolic Syndrome and Its Skeletal Complications. Diabetes Metab Syndr Obes. 2021; 14:241–56. https://doi.org/10.2147/DMSO.S291828 PMID:33500644

3. Winzenrieth R, Ominsky MS, Wang Y, Humbert L, Weiss RJ. Differential effects of abaloparatide and teriparatide on hip cortical volumetric BMD by DXA-based 3D modeling. Osteoporos Int. 2021; 32:575–83. https://doi.org/10.1007/s00198-020-05806-1 PMID:33496831

4. Mi B, Yan C, Xue H, Chen L, Panayi AC, Hu L, Hu Y, Cao F, Sun Y, Zhou W, Xiong Y, Liu G. Inhibition of Circulating miR-194-5p Reverses Osteoporosis through Wnt5a/β-Catenin-Dependent Induction of Osteogenic Differentiation. Mol Ther Nucleic Acids. 2020; 21:814–23. https://doi.org/10.1016/j.omtn.2020.07.023 PMID:32791453

5. Yang S, Wang H, Yang Y, Wang R, Wang Y, Wu C, Du G. Baicalein administered in the subacute phase ameliorates ischemia-reperfusion-induced brain injury by reducing neuroinflammation and neuronal damage. Biomed Pharmacother. 2019; 117:109102. https://doi.org/10.1016/j.biopha.2019.109102 PMID:31228802

6. Xu T, Ge X, Lu C, Dai W, Chen H, Xiao Z, Wu L, Liang G, Ying S, Zhang Y, Dai Y. Baicalein attenuates OVA-induced allergic airway inflammation through the inhibition of the NF-κB signaling pathway. Aging (Albany NY). 2019; 11:9310–27. https://doi.org/10.18632/aging.102371 PMID:31692453

7. Saul D, Gleitz S, Nguyen HH, Kosinsky RL, Sehmisch S, Hoffmann DB, Wassmann M, Menger B, Komrakova M. Effect of the lipoxygenase-inhibitors baicalein and zileuton on the vertebra in ovariectomized rats. Bone. 2017; 101:134–44. https://doi.org/10.1016/j.bone.2017.04.011 PMID:28455215

8. Li SF, Tang JJ, Chen J, Zhang P, Wang T, Chen TY, Yan B, Huang B, Wang L, Huang MJ, Zhang ZM, Jin DD. Regulation of bone formation by baicalein via the mTORC1 pathway. Drug Des Devel Ther. 2015; 9:5169–83. https://doi.org/10.2147/DDDT.S81578 PMID:26392752

9. Yu T, Wang Z, You X, Zhou H, He W, Li B, Xia J, Zhu H, Zhao Y, Yu G, Xiong Y, Yang Y. Resveratrol promotes osteogenesis and alleviates osteoporosis by inhibiting p53. Aging (Albany NY). 2020; 12:10359–69. https://doi.org/10.18632/aging.103262 PMID:32459661

10. Yu T, Xiong Y, Luu S, You X, Li B, Xia J, Zhu H, Zhao Y, Zhou H, Yu G, Yang Y. The shared KEGG pathways between icariin-targeted genes and osteoporosis. Aging (Albany NY). 2020; 12:8191–201. https://doi.org/10.18632/aging.103133 PMID:32380477

11. Xiong Y, Cao F, Chen L, Yan C, Zhou W, Chen Y, Endo Y, Leng X, Mi B, Liu G. Identification of key microRNAs and target genes for the diagnosis of bone nonunion. Mol Med Rep. 2020; 21:1921–33. https://doi.org/10.3892/mmr.2020.10996 PMID:32319614

12. Xiong Y, Chen L, Yan C, Endo Y, Mi B, Liu G. The lncRNA Rhno1/miR-6979-5p/BMP2 Axis Modulates Osteoblast Differentiation. Int J Biol Sci. 2020; 16:1604–15. https://doi.org/10.7150/ijbs.38930 PMID:32226305

13. Dong W, Ye J, Wang W, Yang Y, Wang H, Sun T, Gao L, Liu Y. Self-Assembled Lecithin/Chitosan Nanoparticles Based on Phospholipid Complex: A Feasible Strategy to Improve Entrapment Efficiency and Transdermal Delivery of Poorly Lipophilic Drug. Int J Nanomedicine. 2020; 15:5629–43. https://doi.org/10.2147/IJN.S261162 PMID:32801706

14. Agrawal A, Jørgensen NR. Extracellular purines and bone homeostasis. Biochem Pharmacol. 2021; 187:114425. https://doi.org/10.1016/j.bcp.2021.114425 PMID:33482152

15. Lee S, Liu P, Ahmad M, Tuckermann JP. Leukemia inhibitory factor treatment attenuates the detrimental effects of glucocorticoids on bone in mice. Bone. 2021; 145:115843. https://doi.org/10.1016/j.bone.2021.115843 PMID:33429108

16. Niedermair T, Lukas C, Li S, Stöckl S, Craiovan B, Brochhausen C, Federlin M, Herrmann M, Grässel S. Influence of Extracellular Vesicles Isolated From

Osteoblasts of Patients With Cox-Arthrosis and/or Osteoporosis on Metabolism and Osteogenic Differentiation of BMSCs. Front Bioeng Biotechnol. 2020; 8:615520. https://doi.org/10.3389/fbioe.2020.615520 PMID:33425878

17. Xiong Y, Chen L, Yan C, Zhou W, Yu T, Sun Y, Cao F, Xue H, Hu Y, Chen D, Mi B, Liu G. M2 Macrophagy-derived exosomal miRNA-5106 induces bone mesenchymal stem cells towards osteoblastic fate by targeting salt-inducible kinase 2 and 3. J Nanobiotechnology. 2020; 18:66. https://doi.org/10.1186/s12951-020-00622-5 PMID:32345321

18. Xiong Y, Cao F, Hu L, Yan C, Chen L, Panayi AC, Sun Y, Zhou W, Zhang P, Wu Q, Xue H, Liu M, Liu Y, et al. miRNA-26a-5p Accelerates Healing via Downregulation of PTEN in Fracture Patients with Traumatic Brain Injury. Mol Ther Nucleic Acids. 2019; 17:223–34. https://doi.org/10.1016/j.omtn.2019.06.001 PMID:31272072

19. Sun X, Wei J, Lyu J, Bian T, Liu Z, Huang J, Pi F, Li C, Zhong Z. Bone-targeting drug delivery system of biomineral-binding liposomes loaded with icariin enhances the treatment for osteoporosis. J Nanobiotechnology. 2019; 17:10. https://doi.org/10.1186/s12951-019-0447-5 PMID:30670021

20. Marycz K, Sobierajska P, Roecken M, Kornicka-Garbowska K, Kępska M, Idczak R, Nedelec JM, Wiglusz RJ. Iron oxides nanoparticles (IOs) exposed to magnetic field promote expression of osteogenic markers in osteoblasts through integrin alpha-3 (INTa-3) activation, inhibits osteoclasts activity and exerts anti-inflammatory action. J Nanobiotechnology. 2020; 18:33. https://doi.org/10.1186/s12951-020-00590-w PMID:32070362

21. Li H, Li T, Fan J, Li T, Fan L, Wang S, Weng X, Han Q, Zhao RC. miR-216a rescues dexamethasone suppression of osteogenesis, promotes osteoblast differentiation and enhances bone formation, by regulating c-Cbl-mediated PI3K/AKT pathway. Cell Death Differ. 2015; 22:1935–45. https://doi.org/10.1038/cdd.2015.99 PMID:26206089

22. Zha L, He L, Liang Y, Qin H, Yu B, Chang L, Xue L. TNF-α contributes to postmenopausal osteoporosis by synergistically promoting RANKL-induced osteoclast formation. Biomed Pharmacother. 2018; 102:369–74. https://doi.org/10.1016/j.biopha.2018.03.080 PMID:29571022

23. Xiao Y, Li B, Liu J. MicroRNA-148a inhibition protects against ovariectomy-induced osteoporosis through PI3K/AKT signaling by estrogen receptor α. Mol Med Rep. 2018; 17:7789–96. https://doi.org/10.3892/mmr.2018.8845 PMID:29620276

24. Gómez-Puerto MC, Verhagen LP, Braat AK, Lam EW, Coffer PJ, Lorenowicz MJ. Activation of autophagy by FOXO3 regulates redox homeostasis during osteogenic differentiation. Autophagy. 2016; 12:1804–16. https://doi.org/10.1080/15548627.2016.1203484 PMID:27532863

25. Liao L, Su X, Yang X, Hu C, Li B, Lv Y, Shuai Y, Jing H, Deng Z, Jin Y. TNF-α Inhibits FoxO1 by Upregulating miR-705 to Aggravate Oxidative Damage in Bone Marrow-Derived Mesenchymal Stem Cells during Osteoporosis. Stem Cells. 2016; 34:1054–67. https://doi.org/10.1002/stem.2274 PMID:26700816

26. Feng YL, Jiang XT, Ma FF, Han J, Tang XL. Resveratrol prevents osteoporosis by upregulating FoxO1 transcriptional activity. Int J Mol Med. 2018; 41:202–12. https://doi.org/10.3892/ijmm.2017.3208 PMID:29115382

27. Szklarczyk D, Santos A, von Mering C, Jensen LJ, Bork P, Kuhn M. STITCH 5: augmenting protein-chemical interaction networks with tissue and affinity data. Nucleic Acids Res. 2016; 44:D380–84. https://doi.org/10.1093/nar/gkv1277 PMID:26590256

28. Shannon P, Markiel A, Ozier O, Baliga NS, Wang JT, Ramage D, Amin N, Schwikowski B, Ideker T. Cytoscape: a software environment for integrated models of biomolecular interaction networks. Genome Res. 2003; 13:2498–504. https://doi.org/10.1101/gr.1239303 PMID:14597658

29. Dweep H, Gretz N. miRWalk2.0: a comprehensive atlas of microRNA-target interactions. Nat Methods. 2015; 12:697. https://doi.org/10.1038/nmeth.3485 PMID:26226356

30. Walter W, Sánchez-Cabo F, Ricote M. GOplot: an R package for visually combining expression data with functional analysis. Bioinformatics. 2015; 31:2912–14. https://doi.org/10.1093/bioinformatics/btv300 PMID:25964631